

# Optical Analysis of Nanosecond-Lifetime Plasma Parameters

Parker J. Singletary<sup>1</sup>, Morris B. Cohen, *Senior Member, IEEE*, Mitchell L. R. Walker, Connie Y. Liu<sup>1</sup>, and Cheong Y. Chan

**Abstract**—We present observations and modeling of argon gas at pressures of a few Torr that have been excited with high-voltage pulses (hundreds of volts) on the order of nanoseconds in duration. These tests are motivated by an effort to determine the feasibility of utilizing pulsed argon plasma as a conducting media in a novel antenna configuration. A vacuum chamber is constructed with plate electrodes inserted. An optical observation system is constructed to observe the temporal response. The rise time and fall time of the plasma’s optical emissions, taken as a proxy of the electron density, are measured as a function of pulse voltage and pressure using the captured optical light curve. In addition, spectroscopy measurements are made on a longer time scale. The maximum electron density of the plasma is then inferred through the use of PrismSPECT, a commercially available collisional radiative model, via the line ratio method. Measured pulsed plasmas reached their maximum ionization in as low as 5 ns and recombine in as low as 140 ns. Spectral measurements show that a 1-Torr plasma ionized with 5-ns long pulses had a maximum electron density of  $5.2 \times 10^{20} / \text{m}^3$  and maximum electron temperature of 1.28 eV.

**Index Terms**—Antenna, low frequency (LF), nanosecond ionization, optical measurements, plasma, PrismSPECT, very LF (VLF).

## I. INTRODUCTION

THE work here investigates the response of argon gas to high voltage, nanosecond pulses, as both measured through optical techniques and modeled theoretically. We are exploring the concept of antennas with time-domain matching via rapidly varying conductivity [1]. Extending the time-domain matching concept to plasma will require the development of a plasma that ionizes and recombines in fewer than 30 ns while reaching a high electron density and to conduct radio frequencies up to 1 GHz or an electron density of  $10^{18} / \text{m}^3$ . This application is motivated by scientific and

engineering applications in the very low frequency (VLF) [2] and LF [3] radio bands, where wavelengths are very long. This article serves as a first-order feasibility test to determine whether pulsed argon plasma is a viable medium for the proposed antenna. The time it takes the plasma to reach its maximum level of ionization, recombination time, and electron density capabilities relies heavily on background gas pressure. The experiments in Sections II-B1 and III-A1 are used to determine the effects of gas pressure on the plasma’s ionization with 1-ns resolution. Argon is used as the background gas here as it has a low breakdown voltage at desired working pressures, and its emissions have been well-documented and characterized. The experiments in Section III-B use experimental spectroscopy and radiative modeling to determine the electron density and temperature of the plasma. The results are analyzed in Section IV.

Common methods to obtain time-resolved measurements of plasma electron number density and electron temperature include Langmuir probes, Thomson scattering, laser diode spectroscopy, and optical emission spectroscopy (OES). Langmuir probes have been used to measure transient plasma properties with microsecond resolution [4]. Langmuir probe measurements are subject to noise from high-powered pulses. In addition, the  $I$ - $V$  curves from probe measurements are subject to interpretation: curve slope and saturation current values are extracted manually to calculate electron temperature. Electron density varies strongly as a function of the probe surface area as well, which can vary between measurements due to nonconductive deposits forming on the probe. Thomson scattering is a noninvasive technique, which can yield time-resolved data on the order of 100  $\mu\text{s}$  [5]. This method requires a hot plasma, on the order of 4 eV, and a high electron density, on the order of  $10^{19} / \text{m}^3$ . The plasma generated for this research will not reach these values. Tunable diode laser absorption spectroscopy can be used to track an individual species density and temperature but does not track electron density and temperature well [6]. OES is commonly used to measure plasma parameters either via Stark broadening or the line ratio method [7]. Typical spectrometer measurements are time-averaged and do not yield time-resolved data. A modified spectrometer can be used for time-resolved measurements via nanosecond gating, which is the subject of a concurrent research effort. Following the principles of spectrometer OES, individual line intensities can be tracked with a monochromator and used for time-resolved

Manuscript received June 19, 2019; revised September 13, 2019; accepted November 3, 2019. Date of publication December 9, 2019; date of current version January 20, 2020. This work was supported in part by the Office of Naval Research (ONR) through the Young Investigator Program under Award N00014-15-1-2526 to the Georgia Institute of Technology and in part by the Defense Advanced Research Projects Agency (DARPA) under Award HR0011-16-2-0031 to the Georgia Institute of Technology. The review of this article was arranged by Senior Editor S. Portillo. (*Corresponding author: Parker J. Singletary.*)

P. J. Singletary and M. B. Cohen are with the School of Electrical and Computer Engineering, Georgia Institute of Technology, Atlanta, GA 30313 USA (e-mail: singletarypj@gmail.com).

M. L. R. Walker, C. Y. Liu, and C. Y. Chan are with the School of Aerospace Engineering, Georgia Institute of Technology, Atlanta, GA 30332 USA.

Color versions of one or more of the figures in this article are available online at <http://ieeexplore.ieee.org>.

Digital Object Identifier 10.1109/TPS.2019.2954908

0093-3813 © 2019 IEEE. Personal use is permitted, but republication/redistribution requires IEEE permission. See [http://www.ieee.org/publications\\_standards/publications/rights/index.html](http://www.ieee.org/publications_standards/publications/rights/index.html) for more information.

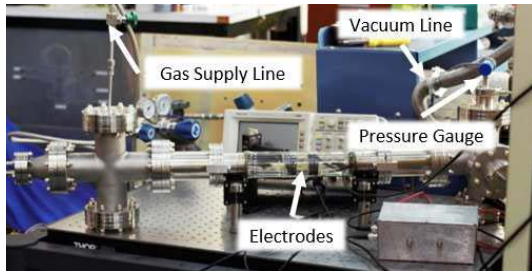


Fig. 1. Plasma vacuum chamber.

line ratio parameter determination [8]. Time-resolved spectra will allow time-resolved parameter determination using many sets of wavelengths, which is a limitation of the monochromator method. Basic OES will be used in this research for preliminary estimates of the argon plasma column's maximum electron density and temperature.

Many studies have focused on the properties of transient plasmas. Pulsed plasma is commonly examined in material processing research, where the focus is on the energy of ions and their effect on various materials [9]. Various studies have examined the effects of pressure and electric field strength on nanosecond pulsed plasma ionization time via particle in cell (PIC) modeling [10], [11]. Plasma recombination rates for glow discharge plasma have also been modeled (PIC, etc.) with experimental verification [12]. The effects of varying voltage pulse rise time on electron temperature and density have been examined experimentally and PIC [13]. The Stark broadening and line ratio methods have been combined to find the temporal evolution of atmospheric pressure argon plasma electron density in response to nanosecond pulses, with a maximum electron density of  $10^{24}/\text{m}^3$  [14], [15]. Time-resolved electron density measurements of parallel plate electrode argon plasma at low pressures have been performed via microwave interferometry [16]. Similar experiments have been used to study nitrogen and carbon dioxide plasma at various pressures [17]. These studies focus on the physical processes behind ionization or recombination. This research will combine both ionization and nanosecond recombination analysis techniques developed by others to fully characterize a nanosecond pulsed plasma.

## II. EXPERIMENTAL CONFIGURATION

### A. Plasma Generation Equipment

The details of the plasma chamber's design and previous versions are described in [18] and reproduced in brief here. Fig. 1 shows the plasma chamber as it was configured for the tests detailed here.

The chamber consists of a 12-in-long, 65.5-mm OD, 4.8-mm wall Pyrex glass tube between two 4.5-in Con-Flat (CF) crosses. The plasma electrodes are positioned in the glass tube for testing. One end of the chamber (downstream) is connected to the vacuum pump, and the other end (upstream) is connected to the mass flow inlet. An Adixen 2121SD roughing pump is used to evacuate the chamber for testing. Chamber pressure is monitored on the vacuum control end by a KJLC 375 gauge controller and KJLC 257 Pirani tube. Accuracy of

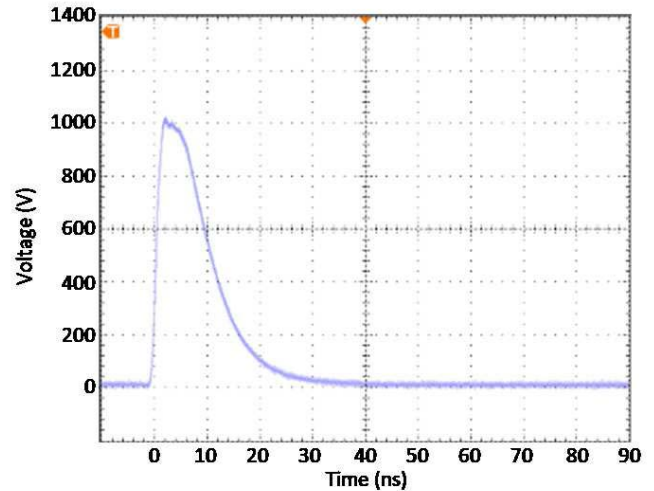


Fig. 2. 1-kV, 10-ns pulse from FID pulser manual.

the gauge in this work's test range is within 10% of reading. Gas flow into the chamber is controlled by an Airgas Y11-215D pressure regulator and a custom flow manifold. The manifold utilizes an MKS 1179A mass flow regulator and an MKS 247D control unit set to provide a flow rate of 200 sccm. The MKS mass flow regulator provides accuracy within 1% of reading. Before each experiment, the roughing pump is used to evacuate the chamber to approximately 10 mTorr. Once the chamber has been evacuated, ultrahigh purity (99.999%) argon is introduced to the system. A bellows valve between the vacuum pump and the chamber is used to manually control chamber pressure. Because the operating pressure is 1 Torr and the evacuation pressure is 10 mTorr, 1% of the gas in the chamber can be considered impurities. To limit further impurities in the system, the authors took care to utilize materials approved for vacuum use that have a low rate of outgassing.

An FID GmbH (FID) (FPG 1-50NM100A) high-voltage pulse generator is used to generate nanosecond-pulsed plasma. This unit can supply pulses from 500 to 1000 V with full-width at half-maximum (FWHM) widths from 5- to 100-ns FWHM and up to 50-kHz repetition frequency into a 75- $\Omega$  load. The pulses from this unit are designed to approximate square waveforms but, at these speeds, the rise and fall of the pulses are noticeable so the pulse is not a clean square pulse. Fig. 2 shows a 1-kV, 10-ns long pulse trace from the FID pulse generator's manual. A voltage divider circuit is used in conjunction with a Tektronix DPO5104B oscilloscope to monitor the voltage supplied to the electrodes. Fig. 3 shows the configuration of the electrode circuit. Fig. 4 shows a 5-ns pulse from the pulser while feeding square electrodes at 1.8-cm gap length with 1-Torr argon in the chamber, measured through the voltage divider circuit. The measured waveform is limited by the 2-GHz resolution of the oscilloscope. The expected amplitude for this scenario is 10 V. The 20% reduction in measured amplitude is a result of imperfect impedance matching.

Two sets of electrodes were manufactured for this work. Fig. 5 shows the rectangular anodized aluminum electrodes (2.54 cm  $\times$  3.81 cm) with  $0.50 \pm 0.01$ -cm gap spacing. The

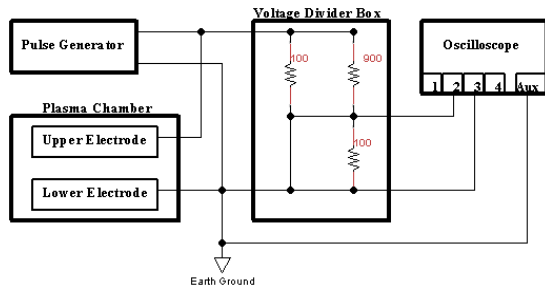


Fig. 3. Ionization circuit schematic.

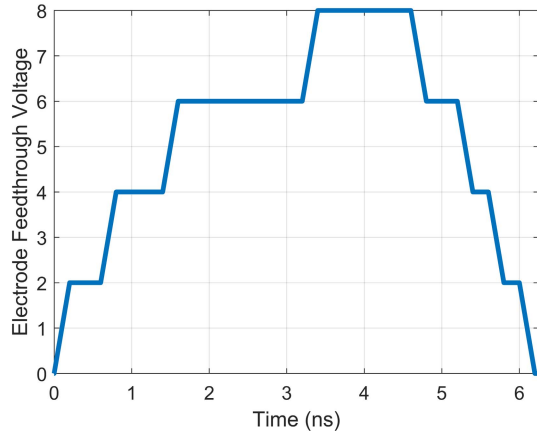


Fig. 4. Voltage measurement at electrode feedthrough. 5-ns, 1000-V pulse feeding rectangular electrodes with 1.8-cm gap and 1-Torr chamber pressure.



Fig. 5. Rectangular electrodes at 0.5-cm gap spacing.

rectangular electrodes were mounted on G10 epoxy laminate brackets. These were reconfigured to have a 1.8-cm gap for the light curve measurements. Fig. 6 shows the rivet electrodes with  $1.00 \pm 0.01$ -cm gap spacing. These were manufactured from 5/32" diameter aluminum round-top rivets (McMaster-Carr 97482A211) mounted on MACOR ceramic brackets. Early experiments with rectangular electrodes were prone to arcing. These smaller electrodes generated more stable, consistent plasma columns. The rivet electrodes were utilized in the spectrometer measurements. Fig. 7 shows the rivet electrodes being supplied with 1 ns, 1-kV pulses to ionize argon at 1 Torr.

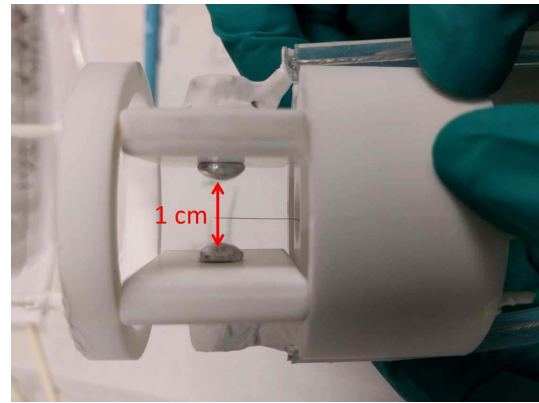


Fig. 6. Rivet electrodes at 1-cm gap spacing.

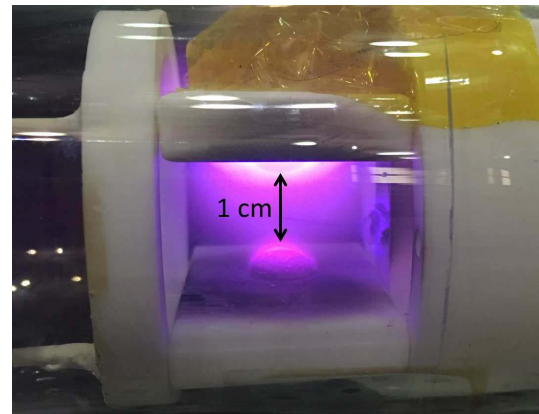


Fig. 7. Rivet electrodes with 1-kV pulsed argon plasma.

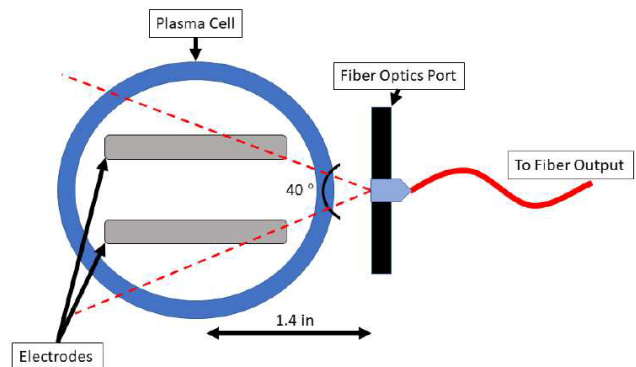


Fig. 8. Optical collection port schematic, courtesy of Chan [18]. The fiber optics port is a Thorlabs F240SMA-780 collimator, and FP1000ERT multimode fiber connects the port to the photodiode.

### B. Plasma Analysis Instrumentation

Both a photodetector and a spectrometer were used to analyze test plasmas. Fig. 8 shows the layout of the electrodes and the optical collection area. The fiber optic output is connected to either the spectrometer or the photodetector. Images of the plasma at each stage of its lifetime would provide qualitative insight into discharge development. To image a plasma that is changing at nanosecond timescales would require a camera with a frame rate of  $\sim 1$  billion frames/s

and high sensitivity. Such a camera was not available for this study so that other techniques were used to capture time variation.

1) *Photodetector*: Photodetector measurements are used to determine how long it takes the experimental plasma to reach its peak ionization when voltage pulses are applied, and how long it takes the plasma to recombine. The conceptual time-domain matched antenna described in Section I utilizes segments with time-varying conductivity, a property that nanosecond-pulsed plasma can provide. The segments of this plasma antenna must ionize and recombine in fewer than 30 ns, reaching a sufficient electron density to support radio frequencies up to 1 GHz ( $N_e = 10^{18} / \text{m}^3$ ). It is necessary to understand the effect of all experimental conditions (gas pressure, gas type, and pulse voltage) on the plasma's ionization and recombination times to determine whether or not it can support the conceptual antenna. A Thorlabs APD430A2 variable-gain avalanche photodetector is used to record total optical output of the plasma as the plasma is modulated or pulsed. This unit detects photons with wavelengths 200–1000 nm, outputting a voltage corresponding to the intensity of light detected. The photodetector is connected to a Tektronix DPO5104B oscilloscope to record voltage traces as a function of time. These traces, henceforth referred to as “light curves,” are recorded via a LabView program provided by Tektronix. Fig. 9 shows a light curve recorded from a plasma excited with a 5-ns, 700-V pulse with 1-Torr argon. The vertical axis is the photodetector output voltage, while the horizontal axis is time. Three parts of these light curves yield information about the rapidly ionized plasma that we explore in more detail: peak optical output, rise time, and fall time. PrismSPECT simulations showed a positive relationship between integrated light intensity and ionization fraction. Thus, a peak in the optical output curve indicates that the plasma's ionization fraction has reached a maximum. Therefore, its electron density has reached a maximum. There is an inherent delay between changes in ionization fraction and emitted light, so the timing of the light curve measurements is not perfectly indicative of exactly when the plasma reached its maximum ionization fraction. Rise and fall times for a light curve are typically measured as the time it takes the magnitude of the curve to increase from 10% of its maximum amplitude to 90% of its maximum amplitude. Here, we define rise time as the time it takes the magnitude of the light curve to increase from 10% of its maximum amplitude to 100% its maximum amplitude. This change in definition is appropriate in this instance because we are interested in the time the plasma takes to reach its highest ionization fraction when a voltage pulse is applied. Noise from the pulse generator and ambient sources coupled into the measurement equipment. The effects of the noise are apparent in Fig. 9 in the “Raw APD Output” curve. The noise made fall time calculations difficult to directly calculate. Measurements of the noise introduced to the optical equipment were performed by measuring photodiode output voltage with the optical input shuttered while the plasma was pulsed. The measured noise amplitude was consistent with the fluctuations in the optical measurements. We applied a moving-average smoothing function to the decreasing section of the curve to

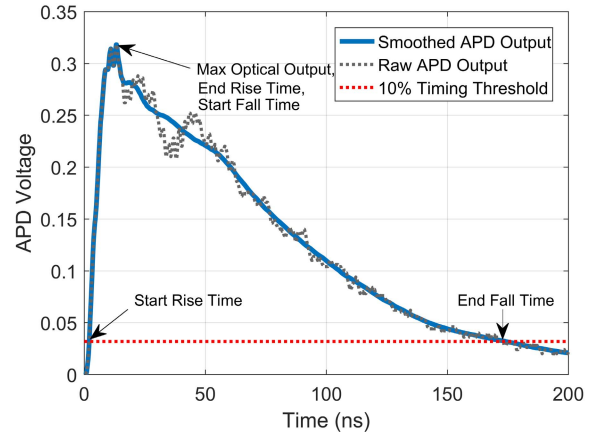


Fig. 9. Raw APD output and smoothed APD output; response to 5-ns, 700-V pulse.

ameliorate these effects. This smoothing introduced an average of 3 ns of error on fall time calculations.

2) *Spectrometer*: An Ocean Optics HR4000CF-UV-near-infrared response (NIR) asymmetric crossed Czerny-Tuner spectrometer is used to collect spectral data. This spectrometer has a wavelength range of 200–1100 nm with an FWHM resolution of 0.75 nm. Each time the spectrometer is used, its wavelength axis is calibrated through the methods described in detail in [18]. The wavelength axis is calibrated using a light source with well-characterized emission lines. In this case, we used an Ocean Optics HG-1 mercury vapor lamp. The lamp is connected to the spectrometer directly via fiber optic cable, and its spectra are measured. A MATLAB algorithm is used to apply corrections from the calibration measurements to measured plasma data. The intensity axis calibration can be a relative or absolute calibration. Absolute calibration provides a conversion between the analog-to-digital units used in a spectrometer to a power density, while a relative calibration accounts only for the spectral sensitivity [7]. An absolute calibration provides more information about the plasma's spectra but is difficult to perform. The relative calibration method focuses only on the shape of the measured spectra and is sufficient for the line ratio method.

### III. RESULTS

#### A. Light Curves

For this set of measurements, the plasma was excited using the rectangular electrodes at a gap length of 1.8 cm powered by the FID pulser, operating at 5-ns pulsewidth and 10-kHz pulse repetition frequency. Pulse amplitude was varied from 500 to 1000 V in 100-V increments. Gas pressure was varied from 200 to 2200 mTorr in 200-mTorr increments. Light curves were recorded for each pressure and voltage combination. Fig. 10 shows the effects of varying ionizing pulse voltage amplitude on peak optical output. As expected, higher ionizing voltages yield higher peak optical output. Fig. 11 shows the effects of varying background gas pressure. Varying pressure changes both the fall and rise times as well as the maximum optical output. Higher pressures at this gap size resulted

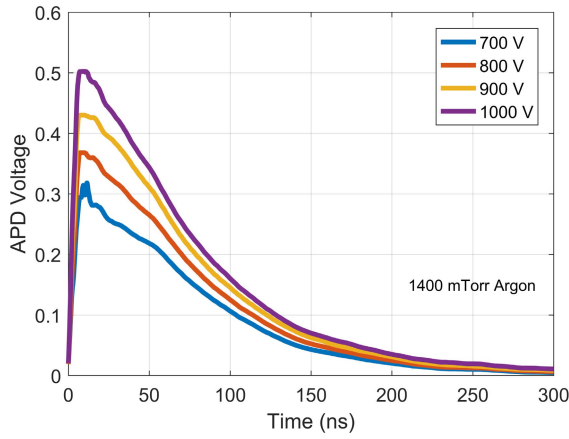


Fig. 10. Smoothed light curves with fixed pressure, varying 5-ns ionizing voltage pulse amplitude.

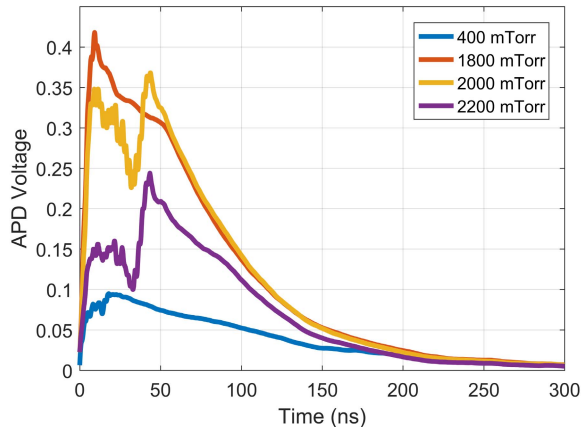


Fig. 11. Smoothed light curves with 5-ns, 800-V ionizing voltage, as a function of pressure.

in double peaks not seen at lower pressures. Peak optical output increased with pressure from 200 to 1800 mTorr. At pressures above 1800 mTorr, peak optical output decreased with pressure.

1) *Pressure–Voltage Sweep*: A pressure–voltage sweep is created by recording light curves at a range of pressures and ionizing voltages. Maximum photodetector output voltage, rise time, and fall time are extracted from the light curves. Fig. 12 displays the maximum photodiode output sweep. Peak optical output always increases when ionization pulse amplitude is increased at a given pressure. Peak optical output is highest between 1400 and 2000 mTorr.

Fig. 12 shows that there is no ionization for lower amplitude voltage pulses as pressure is increased. The Paschen curve predicts breakdown voltage for a given gas, pressure, and electrode gap length. The equation for the Paschen curve is  $V_B = (Bpd / (\ln(Apd) - \ln[\ln(1 + (1/\gamma_{SE}))]))$ , where  $V_B$  is the breakdown voltage.  $A$  and  $B$  are the gas-specific fit parameters.  $\gamma_{SE}$  is the second Townsend coefficient, which is dependent on electrode material [19]. The Townsend coefficient is often unknown and can be combined with the  $A$  fit parameter, becoming  $A'$ , reducing the Paschen curve

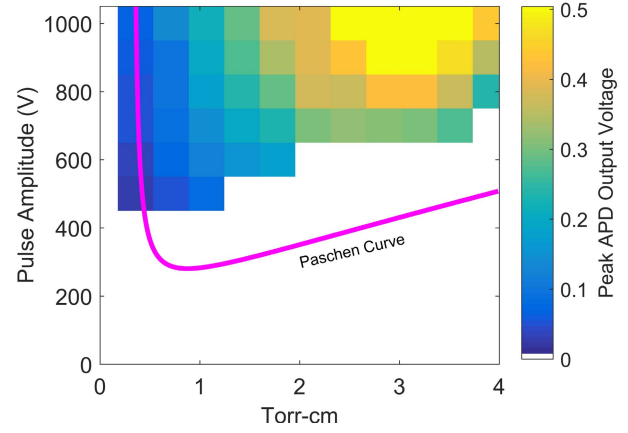


Fig. 12. Peak optical output sweep with Paschen curve overlay at 1.78-cm gap length and 200–2200-mTorr test pressure range.

equation to  $V_B = Bpd / (\ln(A'pd))$ .  $A'$  and  $B$  are determined experimentally. Published values of  $A'$  vary between 2.64 and 3.57 cm-Torr, and  $B$  between 133 and 320 V/cm-Torr for argon [20].  $A' = 3.1$  cm-Torr and  $B = 320$  V/cm-Torr provided the best fit. By multiplying the electrode gap distance by each test pressure, the pressure–voltage sweep plots can be compared to the Paschen curve, which is overlaid in Fig. 12. Differences in experimental design result in significant deviations from the typical Paschen curve: measured threshold voltages were 200 to 300 V above theoretical threshold voltages. Typical Paschen curve experiments are performed with dc ionizing voltages and low-capacitance pin electrodes. Here, nanosecond pulses powered high-capacitance square electrodes. Oscilloscope readings of the ionization feed show the voltage pulses reflecting back and forth in the cable between the electrodes and the pulse generator. Thus, the full potential of each pulse is not utilized in the ionization process. This phenomenon is seen in transmission line theory with transient pulses. The voltage feed lines are terminated in a complex impedance load, with both the capacitance from the square electrode design and the resistance from the anodized layer on the electrodes contributing to the reflections. Performing this test with dc ionizing voltage should result in a Paschen curve fit coefficients similar to those seen in other experiments, allowing steady-state conditions to be met. Because the Paschen curve, in general, applies to dc plasma, this portion of the study provides little insight into the plasma's properties. Rather, this exercise served as a basic verification that experimental plasma tracks typical capacitively coupled plasma (CCP) behavior. Fig. 13 displays the rise time sweep measurement results. Rise time varied from the 30-ns range at 200 mTorr, down to the 5-ns range between 1200 and 1800 mTorr. At pressures above 2000 mTorr, rise time increased to the 40-ns range. The increase in rise time was caused by the double peak effect shown in the light curve plots. Fig. 14 displays the fall time sweep measurement results. Fall time varied from the 300-ns range at 200 mTorr to the 140-ns range at 2200 mTorr. The decreasing fall time as pressure increases is expected due to the linear relationship between pressure and collision frequency. As collision frequency is increased, electrons in the plasma lose their energy more

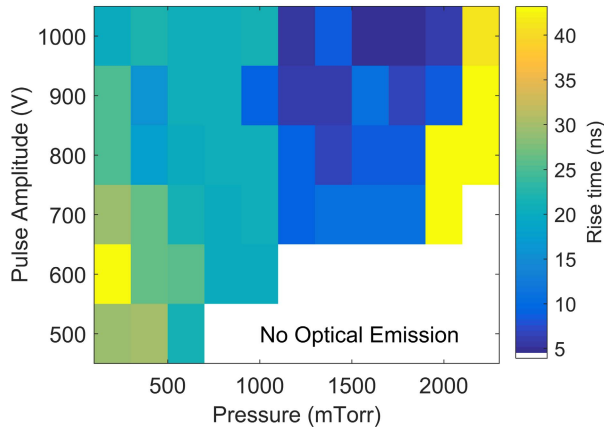


Fig. 13. Rise time with 5-ns ionization pulse at 1.78-cm gap length as a function of background pressure and electrode voltage pulse amplitude.

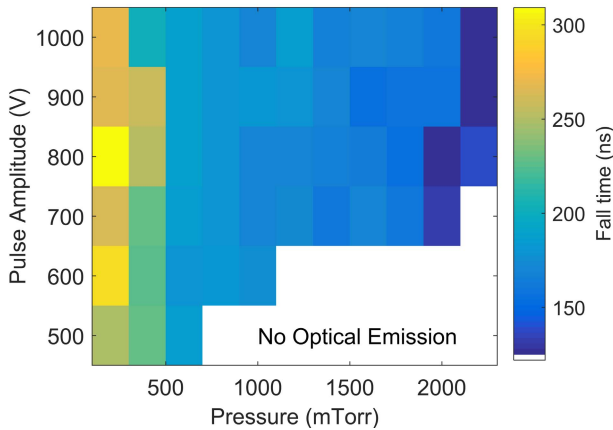


Fig. 14. Fall time with 5-ns ionization pulse at 1.78-cm gap length as a function of background pressure and electrode voltage pulse amplitude.

frequently due to collisions with other electrons, ions, and neutrals. Thus, an increase in collision frequency causes faster recombination.

### B. Pulsed Spectrometer Measurements

The plasma analyzed here was generated by the FID pulsed voltage source with 1-kV, 5-ns pulses at a pulse repetition frequency of 50 kHz, using argon at 1 Torr as the background gas. Because the spectrometer's minimum integration time is 30 ms, it captures many pulses of light during each scan. The integration time on the spectrometer is set to 150 ms for these tests. Increasing the integration time increases the SNR of the spectrometer data. This was necessary for these measurements due to the relatively low intensity of the Ar II lines. This results in the averaged spectra of approximately 7500 pulses per scan. 20 scans are collected and averaged for each test condition. Fig. 15 shows the results of this measurement. National Institute of Standards and Technology (NIST) data and PrismSPECT simulations show that Ar I is the predominant species for plasma with strong lines concentrated around 800 nm such as this one.

The spectra measurements represent the average spectra over the plasma's lifetime. Because the peak emissions are

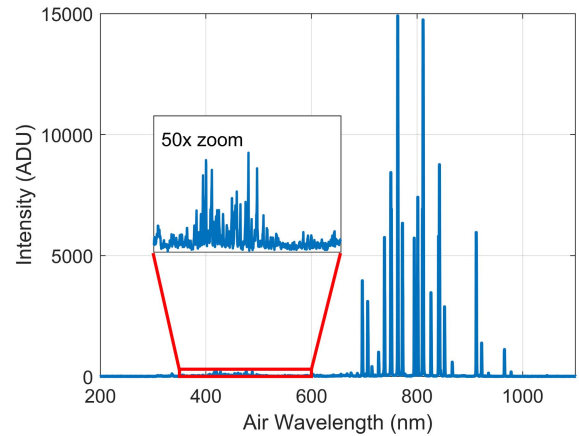


Fig. 15. Measured spectra from 5-ns, 1-kV pulsed, 1-Torr argon plasma with 50 $\times$  magnified spectra from 350 to 600 nm.

much brighter than the average emission level in each pulse, we assume that the average spectra are representative of the plasma at its maximum level of ionization. As the plasma is ionized and recombines, it emits light at wavelengths corresponding to its properties at each point in its lifetime. Thus, a single pulse emits light at a variety of spectra as a function of time. While measuring the spectra at each point in time would be ideal for determining the evolution of its properties, this is no easy task and would require a much more sophisticated set of equipment than what was used. Electron temperature and electron density values inferred in this research yield a first-order estimate of the maximum values of these parameters as the plasma is pulsed. If estimated maximum electron density values are within two orders of magnitude of the desired electron density ( $10^{18}/\text{m}^3$ ), it will provide motivation for a transient study with high time resolution.

## IV. COLLISIONAL RADIATIVE MODEL

In this section, we utilize a theoretical model to infer the plasma properties (namely, electron temperature and density) based on the spectrometer measurements. These properties can be inferred through analysis of the intensity of light emitted from the plasma at individual wavelengths. The intensity of light at each of the wavelengths is a function of gas density and the degree of ionization in the plasma. The peak intensity of one line can be divided by that of another, yielding a "line ratio." Line ratios vary with the degree of ionization as well. Line ratios are calculated for experimental plasmas and compared to models to determine experimental plasma parameters. As it is a ratio of intensities, line ratio calculations do not need an absolute calibration. Radiative models take a plasma's background gas and other experimental parameters into account to generate theoretical spectra, calculating electron density concurrently. The experimental line ratio is compared to that of a number of theoretical plasmas to determine the experimental plasma's parameters. PrismSPECT is a commercially available radiative model used to synthesize spectra, which will be used to apply the line ratio method to experimental data.

### A. PrismSpect Simulations

PrismSPECT is a software package that generates emission simulations of a variety of gases and mixture ratios. The background gas pressure, plasma geometry, and electron temperatures can all be varied in testing. At the simplest level, a radiative model like PrismSPECT determines the density of each excited state for a plasma of a given level of ionization and gas density. The intensity of light emitted at a given wavelength is directly correlated with the population density of the particle's corresponding excited level [7]. Low-pressure ( $10^{-2}$  Torr) plasmas can be modeled with the Corona model, which takes into account only electron impact excitation and radiation from excited electrons. For plasma at our test pressures (1–10 Torr), the more comprehensive collisional radiative model (CRM) is appropriate [21]. PrismSPECT tracks collisional ionization, recombination, deexcitation, photoionization, stimulated recombination, photoexcitation, stimulated emission, spontaneous decay, radiative recombination, dielectronic recombination, autoionization, and electron capture. These processes, along with electron temperature and gas density, are accounted for in a set of rate balance equations used to determine the steady-state density of each species (Ar I, Ar II, etc.) in a plasma. The density of each excited state is directly correlated with the intensity of light at that state's corresponding wavelength. Model spectra are calculated from the state densities. PrismSPECT includes a variety of spectra modeling modes, but low-temperature spectroscopy will be used here. The other modes prove useful for "hot" plasmas seen in fusion reactor experiments such as the ones in [8]. For accurate comparison with experimental measurements, PrismSPECT inputs include gas type, gas pressure, and ambient temperature. Argon gas was used in this article at a pressure of 1 Torr, while the gas temperature in the cell was allowed to vary in the simulation in accordance with the ideal gas law. The plasma geometry is set to zero-width for simplicity and simulation speed. For the line ratio measurements, the pressure is fixed and electron temperature is varied in the nonlocal thermal equilibrium (nonLTE) simulation mode. When a simulation is complete, the spectra and ionization information from each simulation are available, along with individual line intensity information. Simulation results from PrismSPECT are representative of steady-state plasma; however, these can be readily adapted to transient plasma. To observe the effect of electron temperature on the species present in the plasma, PrismSPECT tracks the fraction of the plasma's mean charge resulting from each species, as shown in Fig. 16. Electron density as a function of electron temperature is also tracked, as shown in Fig. 17.

The accuracy of PrismSPECT simulations must be considered when using it to analyze experimental data. Energy level structure and oscillator strengths utilized by PrismSPECT come from NIST experimental data. For strong transitions in LTE simulations, accuracy is expected to be within 1% of actual values. Uncertainty in line strength increases for nonLTE plasmas with external radiation fields or hot electrons, per correspondence with PrismSPECT, but uncertainty levels have been quantified for these conditions. The PrismSPECT

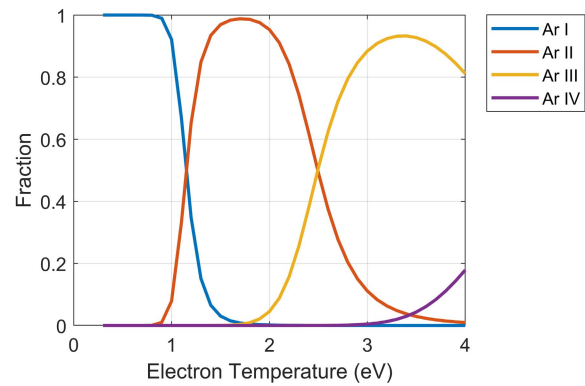


Fig. 16. Mean charge fraction of species as a function of electron temperature at for argon plasma at 1 Torr (PrismSPECT simulation).

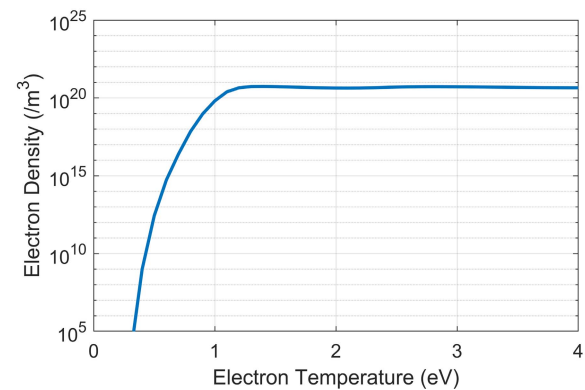


Fig. 17. Electron density as a function of electron temperature for argon plasma at 1 Torr (PrismSPECT simulation).

simulations in this article have an electron temperature resolution of 0.01 eV. The plasma simulated at each plasma temperature has a corresponding electron density. Electron density varies by  $\sim 1\%$  between each tested plasma in the electron temperature range of interest. The spectra from PrismSPECT are representative of steady-state plasma. The transient nature of pulsed plasma could introduce artifacts in measured spectra that are not accounted for in PrismSPECT.

### B. Line Ratio Method

PrismSPECT's built-in line intensity viewer tracks the optical emission resulting from a given transition as plasma simulation parameters are varied. The ratio of one line intensity trace to another yields the plasma's line ratio as a function of electron temperature. To determine the electron transitions generating the plasma's optical emissions, measured emission data were compared to the NIST atomic database [22]. The database displays the known photon wavelengths generated from a given element when ionized. Examination of argon's lines presented an issue: many of the observed wavelengths with strong lines fall within a nanometer of another strong line. The Ocean Optics HR4000 spectrometer has a wavelength resolution of 0.75-nm FWHM. A spectrometer's limited wavelength resolution can cause peak overlap, obscuring the intensity measurement of multiple lines by recording them as a single line with a summed intensity. This effect is problematic

TABLE I  
DETECTED ISOLATED LINES OF ARGON PLASMA

Energy Level	Vacuum Wavelength (nm)
Ar I	738.6014
Ar I	912.2967
Ar II	454.6326
Ar II	465.9205
Ar II	476.4864

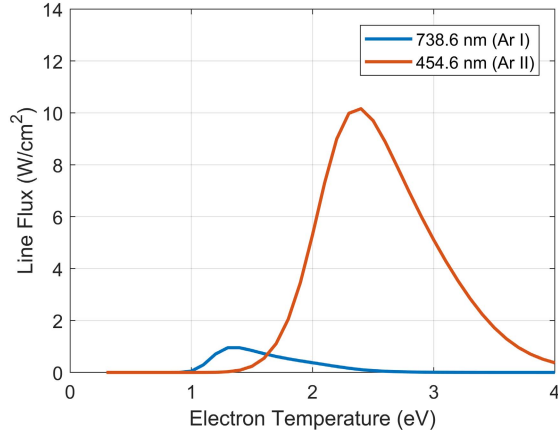


Fig. 18. Argon line intensities as a function of electron temperature.

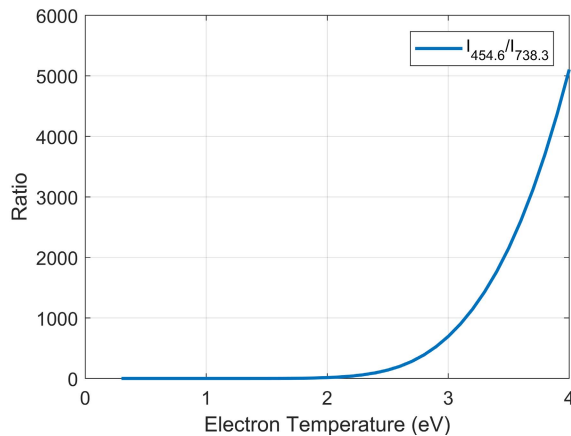


Fig. 19. Ratio of Ar II (454.6 nm) line intensity to Ar I (738.6 nm) line intensity as a function of electron temperature.

for the line ratio method, which relies on peak values of individual lines. The list of candidate lines was narrowed down by selecting only isolated lines ( $\sim 2$  nm away from other lines) in the NIST data. Neutral (Ar I) and singly ionized (Ar II) lines were detected. A comparison of line intensities between the two species is a good indicator of the plasma's degree of ionization, so lines of both species are chosen for comparison to simulated line ratios. The chosen wavelengths are listed in Table I.

Fig. 18 shows the evolution of two line intensities as electron temperature is varied, and Fig. 19 shows the evolution of the ratio of the two selected lines. To determine the electron temperature of the experimental plasma, its line ratio for a given pair of lines is calculated and matched to the simulated data. Multiple ratios will be tracked, and

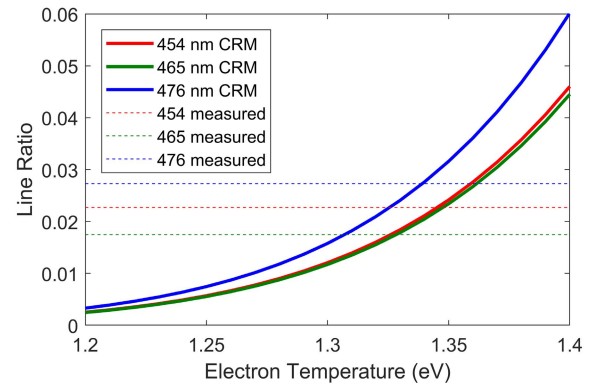


Fig. 20. Ratio of Ar II line intensity to 738.3-nm Ar I line intensity from PrismSPECT compared to 5-ns pulsed plasma line ratio.

their resulting electron temperatures and densities will be averaged.

1) *Nanosecond Pulsed Plasma Line Ratio*: For this test, PrismSPECT's line ratio simulations indicate an electron temperature between 1.23 and 1.34 eV with a standard deviation of 0.06 eV. The mean electron temperature is 1.31 eV, and the average electron density is  $5.2 \times 10^{20}/\text{m}^3$ . Fig. 20 displays the experimental line ratios (dotted lines) compared to the simulated line ratios from PrismSPECT (solid lines). This figure shows the ratios of the three selected Ar II lines to the 738.6-nm Ar I line. Ratios of Ar II were calculated with respect to the Ar I line at 912.2 nm with similar results.

## V. CONCLUSION

A CCP argon plasma's ionization and recombination times were successfully measured for a variety of pressures and ionizing voltages. In response to the high-powered pulses (up to 1 kV), the plasma reached its peak ionization levels in times as low as 10 ns. The plasma recombined in  $\sim 140$  ns in the higher pressure tests. This response time can speed up further with higher pressures, which will require higher amplitude pulses. The higher pressure tests yielded light curves with double emission peaks, the cause of which needs to be investigated further. The pulsed plasma's parameters at the maximum ionization were determined with the line ratio method and PrismSPECT to be on the order of  $10^{20}$  electrons/ $\text{m}^3$ . This result is higher than what was measured via interferometry ( $O \sim 10^{16}/\text{m}^3$ ) under similar conditions (3-Torr, 790-V, 3-ns pulsewidth) [16]. It is difficult to directly compare these experiments, however, due to differences in electrode size, shape, and gap length. The time-averaged spectra could contribute to error in our electron density measurement as well. While the line ratio method allowed the calculation of electron density and temperature for the nanosecond plasma, the presented values must be approached with caution as they are an amalgamation of many sets of spectra. The measurements detailed in this article serve as a feasibility test for pulsed argon plasma as a medium for the proposed variable-conductivity antenna. While the benchmark of recombination in under 30 ns was not met, the results from these experiments suggest

that further testing at higher pressures may yield an argon plasma with high enough conductivity and speed to prove useful in the proposed antenna scheme. A time-resolved set of spectral measurements will better represent the behavior of the transient plasma parameters.

## REFERENCES

- [1] L. A. Thompson, "Broadband electrically short transmitters via time-varying antenna properties," M.S. thesis, Georgia Inst. Technol., Atlanta, GA, USA, 2017.
- [2] M. B. Cohen, U. S. Inan, M. Gołkowski, and N. G. Lehtinen, "On the generation of ELF/VLF waves for long-distance propagation via steerable HF heating of the lower ionosphere," *J. Geophys. Res., Space Phys.*, vol. 115, pp. 1–14, Jul. 2010.
- [3] M. B. Cohen *et al.*, "Broadband longwave radio remote sensing instrumentation," *Rev. Sci. Instrum.*, vol. 89, no. 9, pp. 1–18, 2018, doi: 10.1063/1.5041419.
- [4] J. Alami, J. T. Gudmundsson, J. Bohlmark, J. Birch, and U. Helmerson, "Plasma dynamics in a highly ionized pulsed magnetron discharge," *Plasma Sources Sci. Technol.*, vol. 14, no. 3, pp. 525–531, 2005.
- [5] S. Hübner, J. M. Palomares, E. A. D. Carbone, and J. J. van der Mullen, "A power pulsed low-pressure argon microwave plasma investigated by Thomson scattering: Evidence for molecular assisted recombination," *J. Phys. D: Appl. Phys.*, vol. 45, no. 5, 2012, Art. no. 055203.
- [6] Y. Celik, M. Aramaki, D. Luggenhölscher, and U. Czarnetzki, "Determination of electron densities by diode-laser absorption spectroscopy in a pulsed ICP," *Plasma Sources Sci. Technol.*, vol. 20, no. 1, 2011, Art. no. 015022.
- [7] U. Fantz, "Basics of plasma spectroscopy," *Plasma Sources Sci. Technol.*, vol. 15, pp. S137–S147, Oct. 2006.
- [8] V. H. Chaplin, M. R. Brown, D. H. Cohen, T. Gray, and C. D. Cothran, "Spectroscopic measurements of temperature and plasma impurity concentration during magnetic reconnection at the Swarthmore Spheromak experiment," *Phys. Plasmas*, vol. 16, no. 4, 2009, Art. no. 042505.
- [9] A. Anders, "Fundamentals of pulsed plasmas for materials processing," *Surf. Coat. Technol.*, vol. 183, nos. 2–3, pp. 301–311, 2004.
- [10] F. Iza, J. L. Walsh, and M. G. Kong, "From submicrosecond-to nanosecond-pulsed atmospheric-pressure plasmas," *IEEE Trans. Plasma Sci.*, vol. 37, no. 7, pp. 1289–1296, Jul. 2009.
- [11] H. Y. Kim, M. Gołkowski, C. Gołkowski, P. Stoltz, M. B. Cohen, and M. Walker, "PIC simulations of post-pulse field reversal and secondary ionization in nanosecond argon discharges," *Plasma Sources Sci. Technol.*, vol. 27, no. 5, 2018, Art. no. 055011.
- [12] V. Poterya, J. Glosík, R. Plašil, M. Tichý, P. Kudrna, and A. Pysanenko, "Recombination of  $D_2^+$  ions in the afterglow of a He-Ar- $D_2$  plasma," *Phys. Rev. Lett.*, vol. 88, no. 4, 2002, Art. no. 044802.
- [13] S. Wu, H. Xu, X. Lu, and Y. Pan, "Effect of pulse rising time of pulse DC voltage on atmospheric pressure non-equilibrium plasma," *Plasma Process. Polym.*, vol. 10, no. 2, pp. 136–140, 2013.
- [14] X.-M. Zhu, J. L. Walsh, W.-C. Chen, and Y.-K. Pu, "Measurement of the temporal evolution of electron density in a nanosecond pulsed argon microplasma: Using both Stark broadening and an OES line-ratio method," *J. Phys. D: Appl. Phys.*, vol. 45, no. 29, 2012, Art. no. 295201.
- [15] J. L. Walsh, F. Iza, and M. G. Kong, "Characterisation of a 3 nanosecond pulsed atmospheric pressure argon microplasma," *Eur. Phys. J. D*, vol. 60, no. 3, pp. 523–530, 2010.
- [16] V. Podolsky, A. Khomenko, and S. Macheret, "Time-resolved measurements of electron number density in argon and nitrogen plasmas sustained by high-voltage, high repetition rate, nanosecond pulses," *Plasma Sources Sci. Technol.*, vol. 27, no. 10, 2018, Art. no. 10LT02.
- [17] N. L. Aleksandrov, S. V. Kindysheva, A. A. Kirpichnikov, I. N. Kosarev, S. M. Starikovskaia, and A. Y. Starikovskii, "Plasma decay in  $N_2$ ,  $CO_2$  and  $H_2O$  excited by high-voltage nanosecond discharge," *J. Phys. D: Appl. Phys.*, vol. 40, no. 15, pp. 4493–4502, 2007.
- [18] C. Y. Chan, "Experimental investigation of fast plasma production for the VAIPER antenna," M.S. thesis, Georgia Inst. Technol., Atlanta, GA, USA, 2017.
- [19] W. E. Bowls, "The effect of cathode material on the second Townsend coefficient for ionization by collision in pure and contaminated  $N_2$  gas," *Phys. Rev.*, vol. 53, no. 4, pp. 293–300, 1937.
- [20] R. Massarczyk, P. Chu, C. Dugger, S. R. Elliott, K. Rielage, and W. Xu, "Paschen's law studies in cold gases," *J. Instrum.*, vol. 12, no. 6, 2017, Art. no. P06019.
- [21] X.-M. Zhu and Y.-K. Pu, "Optical emission spectroscopy in low-temperature plasmas containing argon and nitrogen: Determination of the electron temperature and density by the line-ratio method," *J. Phys. D: Appl. Phys.*, vol. 43, no. 40, 2010, Art. no. 403001.
- [22] *NIST Atomic Spectra Database*. Accessed: Feb. 1, 2018. [Online]. Available: [https://physics.nist.gov/PhysRefData/ASD/lines\\_form.html](https://physics.nist.gov/PhysRefData/ASD/lines_form.html)



**Parker J. Singletary** received the B.S. degree in electrical engineering from The Citadel, The Military College of South Carolina, Charleston, SC, USA, in 2015, and the M.S. degree in electrical engineering from the Georgia Institute of Technology, Atlanta, GA, USA, in 2018, where he is currently pursuing the Ph.D. degree in electrical engineering with a focus in electromagnetics.

In 2015, he joined the Low Frequency Radio Group, Georgia Institute of Technology. He received the President's Fellowship from Georgia Tech. Upon graduation in the spring of 2020, he will join Georgia Tech Research Institute (GTRI), Atlanta, as a Research Engineer. He specializes in the areas of plasma antennas, nanosecond pulsed plasma parameter measurements, and plasma finite-difference time-domain (FDTD) modeling.



**Morris B. Cohen** (M'10–SM'19) received the B.S. and Ph.D. degrees in electrical engineering from Stanford University, Stanford, CA, USA, in 2003 and 2010, respectively.

He served as a Research Associate with the Department of Electrical Engineering, Stanford University until August 2013. From August 2012 to 2013, he was concurrently appointed as an AAAS Science and Technology Policy Fellow, serving at the National Science Foundation. In Fall 2013, he joined the School of Electrical Engineering, Georgia Institute of Technology, Atlanta, GA, USA as an Assistant Professor and has been an Associate Professor with tenure since August 2018. His research focuses on low-frequency radio wave generation, propagation, detection, and data science. He is currently a President-Elect with the Atmospheric and Space Electricity Section, American Geophysical Union. He has authored or coauthored 65 journal articles.

Dr. Cohen is a 2014 Winner of the Santimay Basu Prize by the International Union of Radio Science, which is given once per three years to an under-35 scientist. He also won the 2015 Office of Naval Research (ONR) Young Investigator Winner, the 2017 NSF CAREER Award, and the Georgia Tech's Junior Faculty Teaching Excellence Award in 2018. He is an Associate Editor of *Radio Science*.



**Mitchell L. R. Walker** received the Ph.D. degree in aerospace engineering from the University of Michigan, Ann Arbor, MI, USA, in 2004, with a focus on experimental plasma physics and advanced space propulsion.

He is currently a Professor of aerospace engineering and the Associate Chair of Graduate Studies with the Georgia Institute of Technology, Atlanta, GA, USA, where he directs the High-Power Electric Propulsion Laboratory. His training includes rotations with Lockheed Martin, Sunnyvale, CA, USA,

and the NASA Glenn Research Center, Cleveland, OH, USA. In 2005, he founded the Electric Propulsion Program at the Georgia Institute of Technology. He has authored more than 120 journal articles and conference papers in the fields of electric propulsion and plasma physics. His primary research interests include both experimental and theoretical studies of advanced plasma propulsion concepts for spacecraft and fundamental plasma physics. His research activities include Hall effect thrusters, gridded ion engines, magnetoplasmadynamic thrusters, diagnostics for plasma interrogation and thruster characterization, vacuum facility effects, helicon plasma sources, plasma-material interactions, and electron emission from carbon nanotubes.

Dr. Walker is an Associate Fellow of AIAA and the Chair of the AIAA Electric Propulsion Technical Committee, where he delivered expert witness testimony In-Space Propulsion: Strategic Choices and Options to the Space Subcommittee Hearing—House of Representatives, Washington, DC, USA, in 2017, helping guide national investments in electric propulsion technology. He is a recipient of the Georgia Power Professor of Excellence Award, the AIAA Lawrence Sperry Award, the Air Force Office of Scientific Research Young Investigator Program Award, and the NASA Faculty Fellow Award. He served as an Associate Editor for the American Institute of Aeronautics and Astronautics (AIAA) and has been serving on the Editorial Board of *Frontiers in Physics and Astronomy and Space Sciences Plasma Physics* since 2015. He was a Participant in the 2014 U.S. National Academy of Engineering U.S. Frontiers of Engineering Symposium. In 2015, he was the Co-Organizer for a focus session at the Frontiers of Engineering Symposium.



**Connie Y. Liu** received the B.S. degree in aerospace engineering from the Massachusetts Institute of Technology, Cambridge, MA, USA, in 2015, and the M.S. degree in aerospace engineering and the Ph.D. degree in aerospace engineering, with a focus on electric propulsion and pulsed plasmas, from the High-Power Electric Propulsion Laboratory, Georgia Institute of Technology, Atlanta, GA, USA, in 2016 and 2019, respectively.

She is currently a Propulsion Development Engineer with Space Exploration Technologies, Hawthorne, CA, USA. She specializes in the areas of electric propulsion, rocket combustion propulsion, and nanosecond pulsed plasmas.



**Cheong Y. Chan** received the B.A. degree in physics from the University of California at Berkeley, Berkeley, CA, USA, in 2011, the M.Sc. degree in physics from Yale University, New Haven, CT, USA, in 2013, and the M.Sc. degree in aerospace engineering from the Georgia Institute of Technology, Atlanta, GA, USA, in 2017.

He is currently a System Engineer with Northrop Grumman Innovation System, Northridge, CA, USA, specializing in advanced exploration missions and robotic servicing.